Title

An Age-Specific Atlas for Delineation of White Matter Pathways in Children Aged 6-8 Years

Author names and affiliations

Arthur Spencer[a]*, Hollie Byrne[a], Richard Lee-Kelland[b], Sally Jary[b], Marianne Thoresen[b,c], Frances Cowan[b,d], Ela Chakkarapani[b], Jonathan C.W. Brooks[a,e].

[a]Clinical Research and Imaging Centre, University of Bristol, Bristol, UK
[b]Faculty of Health Sciences, Translational Health Sciences, Bristol Medical School, University of Bristol, Bristol, UK
[c]Faculty of Medicine, Institute of Basic Medical Sciences, University of Oslo, Oslo, Norway
[d]Department of Paediatrics, Imperial College London, London, UK
[e]School of Psychological Science, University of Bristol, Bristol, UK
*Corresponding author; arthur.spencer@bristol.ac.uk; Clinical Research and Imaging Centre, University of Bristol, 60 St Michael´s Hill, Bristol, BS2 8DX

Declarations of interest: none

CRediT authorship contribution statement:

Arthur Spencer: Conceptualisation; data curation; formal analysis; methodology; software; validation; visualisation; writing – original draft.
Hollie Byrne: Data curation; investigation.
Richard Lee-Kelland: Data curation; investigation.
Sally Jary: Investigation.
Marianne Thoresen: Investigation.
Frances Cowan: Investigation.
Ela Chakkarapani: Funding acquisition; methodology; project administration; resources; supervision; validation; writing – review & editing.
Jonathan Brooks: Methodology; resources; supervision; validation; writing – review & editing.

Abstract

Diffusion MRI allows non-invasive assessment of white matter maturation in typical development and of white matter damage due to brain injury or pathology. Reliably attributing diffusion metrics to specific white matter pathways either requires use of lengthy acquisition protocols with numerous diffusion directions, which may be problematic in certain cohorts (e.g. children or adults with mild cognitive impairment), or probabilistic white matter atlases, which allow delineation of white matter tracts without the need to perform tractography, thus eliminating the need for the extensive scans required for modern tractography algorithms. However, given the known age-dependency of developmental change in white matter it may not be optimal to use an adult template when assessing data acquired from children.

This study develops an age-specific probabilistic white matter atlas for delineation of 12 major white matter tracts in children aged 6-8 years. By comparing to fibre tracking in individuals, we demonstrate that this age-specific atlas gives better overall performance than simply registering to the Johns Hopkins University (JHU) adult white matter template in both data acquired from a single cohort on a single scanner (age-specific r = 0.72; JHU r = 0.54) and from a cohort taken from the ABIDE dataset (age-specific r = 0.75; JHU r = 0.72). Accuracy was assessed by comparing estimates of tract-level diffusion metrics, using the age-specific and adult templates, to results of subject-specific tracing. To our knowledge, this is the first publicly available probabilistic atlas of white matter tracts for this age group.

We then use the age-specific atlas to provide evidence for reduced fractional anisotropy in several tracts in children who were treated with therapeutic hypothermia for neonatal encephalopathy at birth and did not have cerebral palsy, compared with controls matched for age, sex and socio-economic status.

Keywords

White matter, Development, Atlas, dMRI, Tractography.

Abbreviations

DWI – diffusion-weighted imaging; FA – fractional anisotropy; NE – neonatal encephalopathy; TH – therapeutic hypothermia.

1 Introduction

Tract-level analysis of diffusion weighted imaging (DWI) data is used extensively to investigate white matter microstructure in both typical (Asato et al., 2010; Hüppi and Dubois, 2006; Lebel et al., 2008) and atypical brain development (for a review, see (Dennis and Thompson, 2013)). In children and adolescents, atypical brain development may lead to physical and intellectual disabilities including e.g. cerebral palsy (CP) (Arrigoni et al., 2016), autistic spectrum behaviours (Ameis and Catani, 2015; Dimond et al., 2019) and attention deficit hyperactivity disorder (Konrad and Eickhoff, 2010).

A widely employed technique to delineate white matter tracts is to segment streamlines generated by tractography (Lawes et al., 2008; Sydnor et al., 2018; Wakana et al., 2007; Wassermann et al., 2010; Zhang et al., 2018), however acquiring accurate tractography requires lengthy scanning protocols (i.e. HARDI) which are susceptible to head motion. Extended scan times can be problematic for some children, especially those with disabilities who would benefit from investigating white matter development (Phan et al., 2018).

Where long scans pose difficulty, shorter sequences can still provide the data required to construct diffusion tensors. Though not optimal, the tensor model offers insight into white matter microstructure by calculating metrics such as fractional anisotropy (FA), mean diffusivity (MD), radial diffusivity (RD) and axial diffusivity (AD) (Assaf and Pasternak, 2008). These metrics are sensitive to changes in the underlying white matter structure, thus are widely investigated in brain development (Dennis and Thompson, 2013; Lebel et al., 2008), as well as having clinical relevance in patient cohorts (Assaf et al., 2019; Assaf and Pasternak, 2008; Horsfield and Jones, 2002). Lacking the high angular resolution data required for tractography, white matter tracts can be delineated by registering to a standard template with a probabilistic atlas of tract locations. However, the widely used Johns Hopkins University (JHU) atlas (Hua et al., 2008) is constructed from adult data. Numerous developmental studies demonstrate white matter alterations continuing into adolescence (Cascio et al., 2007; Hagmann et al., 2010; Lebel et al., 2008; Simmonds et al., 2014), and white matter development varies widely across the brain (Lebel et al., 2019), therefore an atlas constructed from adult scans is by design and definition not representative of children. There are several publicly available age-specific structural templates (Altaye et al., 2008; Fonov et al., 2011; Richards et al., 2016; Sanchez et al., 2012), however none of these provide diffusion data.

Using robust tract reconstruction protocols (Wakana et al., 2007) this study develops an age-specific probabilistic white matter atlas for 12 major tracts in children aged 6-8 years. To assess whether this atlas accurately delineates tracts, we measured both volumetric overlap and the diffusion metrics sampled by the tract mask in comparison with tractography-based tract delineation. We then assess

the utility of this age-specific tract atlas by comparing it to results obtained using an adult atlas (JHU). The atlas is then further validated against an open data source (i.e. different scanner), and against a different tractography algorithm.

As a demonstration of proof of concept, we then investigate tract-level differences in children treated with therapeutic hypothermia (TH) for neonatal encephalopathy (NE) at birth, compared with healthy controls, and compare results obtained using the age-specific atlas to those from the JHU atlas. The children who had TH, do not have CP and are in mainstream education still exhibit significantly reduced performance on cognitive tests (Jary et al., 2019; Lee-Kelland et al., 2020) and have slower reaction times and reduced visuo-spatial processing abilities (Tonks et al., 2019), compared to the healthy controls.

This age-specific atlas provides a method of delineating white matter tracts in children without tractography, thus lending itself to clinical settings, application to large datasets, and research studies involving cohorts who may be averse to long scan times.

2 Material and Methods

2.1 Participants

Ethics approval was obtained from the North Bristol Research Ethics Committee and the Health Research Authority (REC ID: 15/SW/0148). Informed and written consent was obtained from the parents of participants before collecting data. The cohort was made up of 36 healthy children aged 6-8 years with no evidence of neurological disease, originally recruited as controls for a study of the long-term effects of TH ("CoolMRI") on behavioural and imaging outcomes. The 36 controls were split randomly into 28 atlas and 8 validation subjects such that the group were matched for age, sex, socio-economic status (SES) and full-scale intelligence quotient (FSIQ). For the demonstrative case study, data from 33 children treated with TH following NE at birth were compared to the control data. Participant demographics are shown in Section 3.1.

2.2 Image Acquisition

DWI data were acquired with a Siemens 3 Tesla Magnetom Skyra MRI scanner at the Clinical Research and Imaging Centre (CRiCBristol), Bristol, UK. Subjects were placed supine within the 32-channel receive only head-coil by an experienced radiographer, and head movement minimised by means of memory-foam padding. Children wore earplugs and were able to watch a film. A parent was only allowed in the room in exceptional circumstances (i.e. if the child was very nervous). A multiband echo-planar imaging (EPI) sequence was used with the following parameters: TE = 70 ms;

TR = 3150 ms; field of view 192 × 192 mm; 60 slices; 2.0 mm isotropic voxels; phase encoding in the anterior-posterior direction, in-plane acceleration factor = 2 (GRAPPA (Griswold et al., 2002)), through-plane multi-band factor = 2 (Moeller et al., 2010; Setsompop et al., 2012b, 2012a).

For the purpose of data averaging and eddy-current distortion correction, two sets of diffusion weighted images were acquired with b = 1,000 s mm^{-2} in 60 diffusion directions, equally distributed according to an electrostatic repulsion model, as well as 8 interspersed b = 0 images, with one data set acquired with positive phase encoding steps, then repeated with negative steps (so-called, "blip-up", "blip-down"), giving a total of 136 images.

2.3 Quality Control

The quality of the diffusion data was assessed using the EddyQC tool (Bastiani et al., 2019) from FSL (Smith et al., 2004). This provides several measures of the amount of movement and eddy current induced distortion present in the data. For each participant, the root-mean-square of all metrics was calculated, giving a score which increases monotonically with the amount of movement and eddy current distortion. Scans were rejected if their score was more than one standard deviation above the mean of all participants.

2.4 Image Processing & Atlas Construction

DWI data were denoised and corrected for eddy current induced distortions and subject movements using EDDY (Andersson and Sotiropoulos, 2016) and TOPUP (Andersson et al., 2003), part of FSL. Subsequent DWI processing and tractography steps were performed using MRtrix (Tournier et al., 2019). The response function (the DWI signal for a typical fibre population) was estimated from the data (Tournier et al., 2013). The fibre orientation distribution (FOD) was then calculated by performing constrained spherical deconvolution of the response function from the measured DWI signal (Tournier et al., 2007). Deterministic tractography was run in each subject using the "SD Stream" algorithm (Tournier et al., 2012). Streamlines were seeded randomly in the brain and generated with a step size of 0.2 mm, then terminated if the FOD amplitude dropped below 0.2 or the angle between successive steps exceeded 40 degrees. 10 million streamlines were generated, which were then filtered to 1 million using spherical-deconvolution informed filtering of tractograms (SIFT) (Smith et al., 2013) to give better reconstruction of FODs, improving anatomical accuracy.

The process of generating probability maps from the whole-brain tractograms is summarised in Figure 1. White matter tracts were segmented from whole-brain tractograms using the protocols described in (Wakana et al., 2007), whereby regions of interest (ROI) are drawn to include or exclude streamlines passing through them. For a given tract, any streamlines which pass through all inclusion ROIs and no

exclusion ROIs belong to that tract, and all other streamlines are removed. Inclusion and exclusion ROIs were manually drawn in each subject to delineate 12 major fibre tracts: anterior thalamic radiation (ATR); cingulate gyrus part of the cingulum (CG); hippocampal part of the cingulum (CH); cortico-spinal tract (CST); forceps major (Fmajor); forceps minor (Fminor); inferior fronto-occipital fasciculus (IFOF); inferior longitudinal fasciculus (ILF); superior longitudinal fasciculus (SLF); temporal part of the superior longitudinal fasciculus (SLFt); uncinate fasciculus (UF); and the fornix. The locations of ROIs for all tracts apart from the fornix are described in (Wakana et al., 2007), as shown in Figure 2.

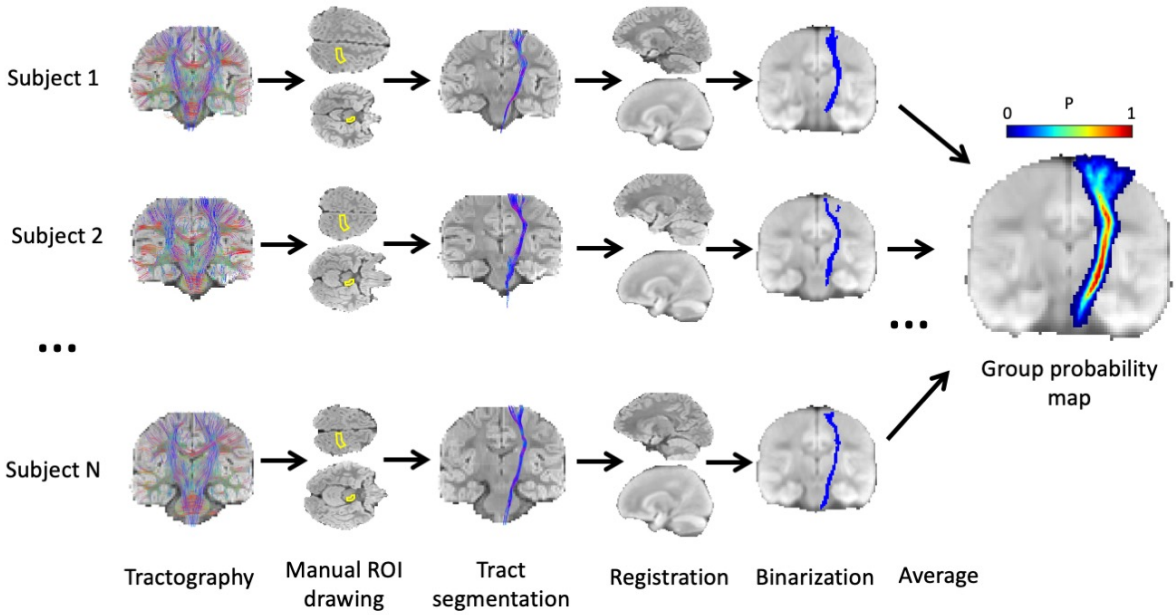

Figure 1: Methodology for generating probabilistic tract maps from whole-brain tractography data, shown here for the corticospinal tract (CST). ROIs were manually drawn in each subject, as defined by (Wakana et al., 2007) (in the case of the CST, inclusion ROIs were drawn in the cerebral peduncle and the primary motor cortex), and tracts were segmented by including streamlines passing through the inclusion ROIs. Streamlines were transformed to standard space (JHU template) and a binary mask was created for each subject indicating all voxels containing streamlines. The average of these masks (across N = 28 subjects) gives the probability map.

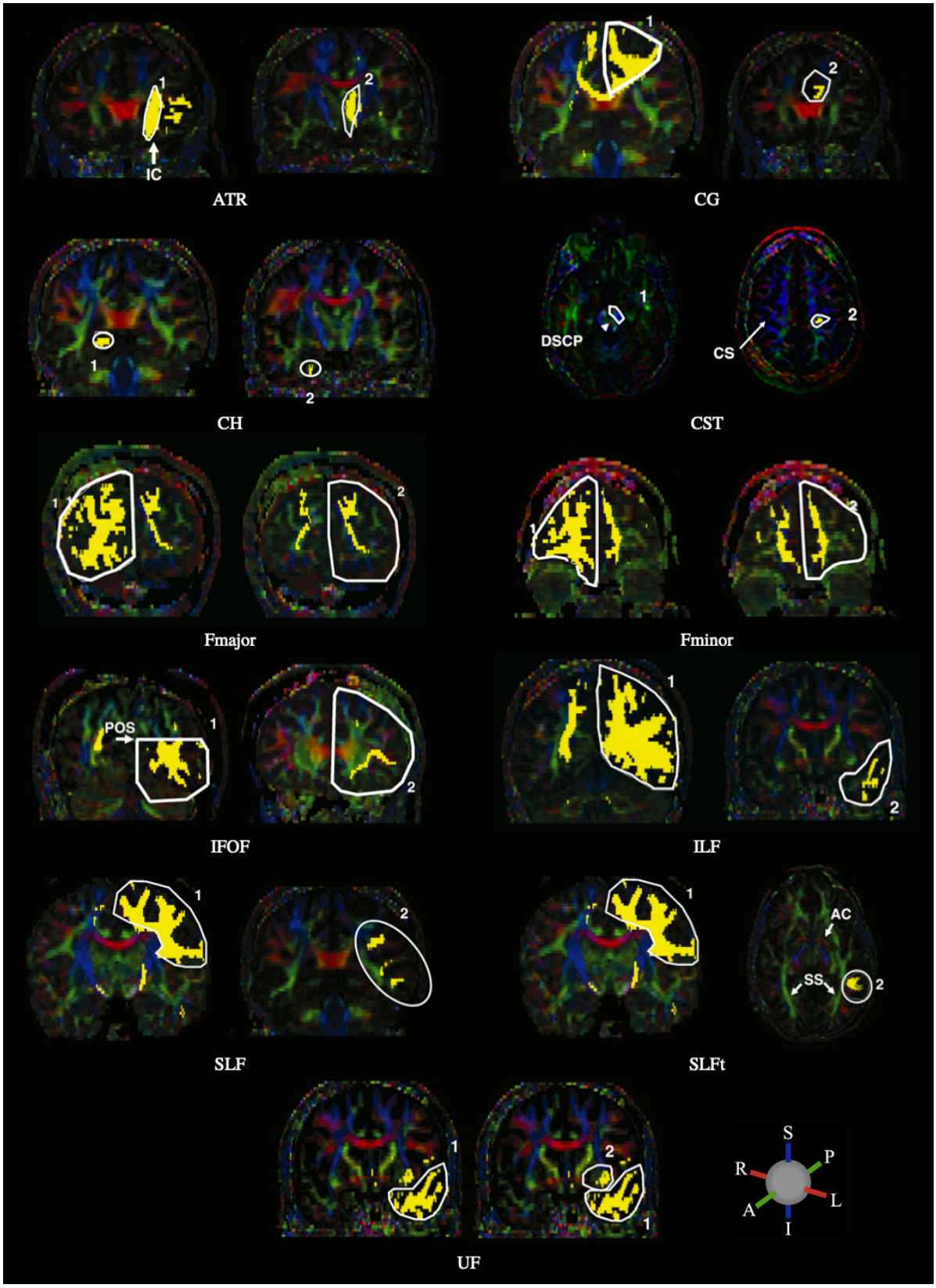

Figure 2: ROIs used to delineate the following major white matter tracts: anterior thalamic radiation (ATR); cingulate gyrus part of the cingulum (CG); hippocampal part of the cingulum (CH); cortico-spinal tract (CST); forceps major (Fmajor); forceps minor (Fminor); inferior fronto-occipital

fasciculus (IFOF); inferior longitudinal fasciculus (ILF); superior longitudinal fasciculus (SLF); temporal part of the superior longitudinal fasciculus (SLFt); uncinate fasciculus (UF). Streamlines are included in a given tract if they pass through both 1 AND 2. The following abbreviations indicate anatomical landmarks used to draw the ROIs: internal capsule (IC); decussation of the superior cerebellar peduncle (DSCP); central sulcus (CS); parieto-occipital sulcus (POS); anterior commissure (AC); sagittal stratum (SS). ROIs are drawn in white with streamlines in yellow, overlaid on FA images with principal diffusion directions indicated by the colour ball; blue = superior-inferior (S-I), green = anterior-posterior (A-P) and red = right-left (L-R). Adapted from (Wakana et al., 2007) with permission from Elsevier.

To delineate the fornix, streamlines were included which pass through the body of the fornix and either of the posterior limbs which project to the hippocampus (Figure 3). These were isolated by first selecting an axial level at the lower edge of the splenium of the corpus callosum, as seen in the mid-sagittal plane (Figure 3, left); in this axial level, the first ROI was drawn around the body of the fornix. Viewing the streamlines which are delineated by the first ROI, additional bilateral ROIs were defined to include only those which project posteriorly from the fornix body (Figure 3, right).

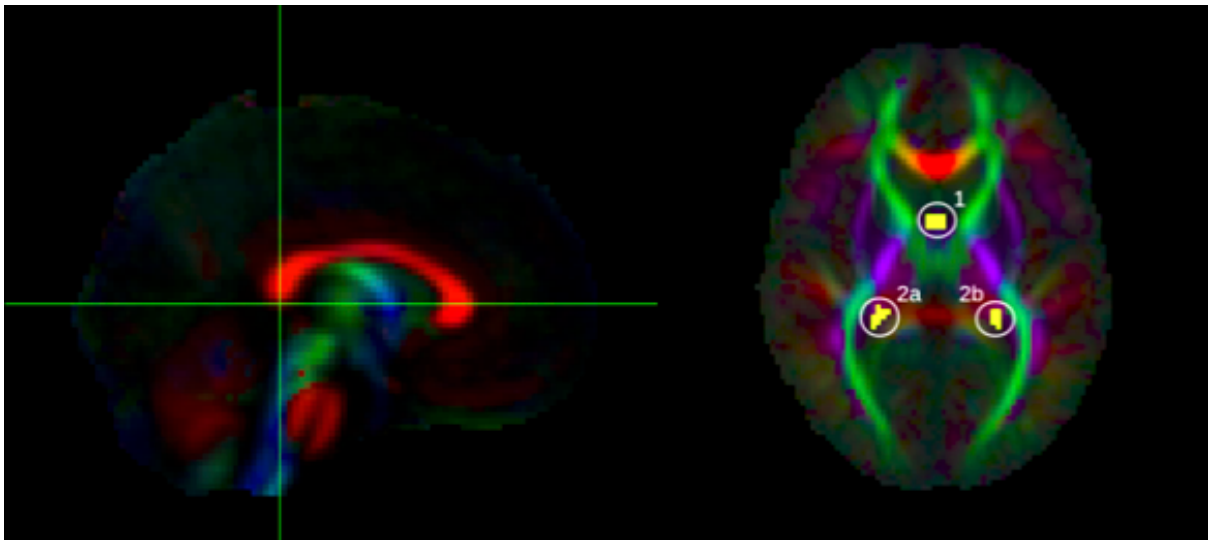

Figure 3: ROIs used to delineate the fornix, shown here on the group FA template. Yellow voxels contain streamlines which pass through the body of the fornix (1) AND bilateral posterior limbs of fornix (2a OR 2b).

For spatial normalisation, the average diffusion weighted image (aDWI), created for each subject by averaging all DWI images, was registered to the JHU aDWI template by 12-degree of freedom affine registration using FSL's FLIRT (Jenkinson et al., 2002). The resulting transformation was then applied to the segmented streamlines. Any voxel containing one or more of these streamlines was then labelled, to create a binary mask for the tract for each individual. The average, across 28 subjects, of

these binary masks was taken to give a probability map for each tract. The aDWI was then created for the group by averaging transformed aDWIs from all 28 subjects, and the group FA image was created from the group-average tensor map.

This atlas is available at Neurovault (https://neurovault.org/collections/LWTAAAST/)[1]. Data is available upon request to the corresponding author.

2.5 Validation

Two datasets were used for validation. The first was made up of 8 subjects drawn randomly from the 36 control participants from CoolMRI. These subjects were scanned using the same scanner and scanning parameters as the remaining 28 subjects used in construction of the atlas. Subject specific tracts were traced in these individuals using the method described in Section 2.4.

The second validation dataset comprises data obtained from the Autism Brain Imaging Data Exchange II[2] (ABIDE) database (Di Martino et al., 2017), available online as part of the International Neuroimaging Data Sharing Initiative. This allows validation using subjects scanned in a different scanner, and with different scanning parameters, in order to alleviate any bias associated with same-site scans. Scans were obtained from 7 subjects, aged 8-9 years. Both typical controls (n = 3) and subjects with autism spectrum disorder (n = 4) were used. Due to data availability the age range of these subjects extends slightly above that of the atlas, however it serves as a test of how well the atlas generalises. These images were acquired on a GE 3T MR750 scanner with an 8-channel head coil using an echo-planar pulse sequence with the following parameters: TE = 84.9 ms; TR = 8500 ms; FoV = 240 mm; 128 x 128 matrix; 68 slices; 1.88 x 1.88 x 2 mm resolution; 61 diffusion directions with b = 1,000 s mm^{-2}; and one b = 0 image. To remove any further bias resulting from the validation data being processed with the same tractography algorithm, tracts in the ABIDE subjects were traced using a deterministic tensor-based algorithm (Basser et al., 2000).

After all tracts were traced in every validation subject, they were nonlinearly registered to the group FA image, constructed from the 28 atlas subjects, using FSL's FNIRT (Andersson et al., 2007). To compare spatial similarity between normalised data we tested the volumetric overlap between the probabilistic atlas (age-specific or JHU) and each individually traced tract by measuring the Dice score (Dice, 1945) over a range of thresholds. The amount of volumetric overlap between the atlas data and the individually traced tract will depend on both i) the quality of registration of the individual to the template, and ii) the agreement between the atlas data and the results from tractography in the

[1] Currently accessible only via this link. Repository will be made public upon publishing.
[2] http://fcon_1000.projects.nitrc.org/indi/abide/abide_II.html

individual. Thus, if the template is a closely matched target for registration, and if the underlying anatomy and diffusion process captured by the atlas is a good match to the validation subjects, we expect the Dice scores to be high.

We then assessed the ability of the atlas to reproduce individually traced DWI metrics by calculating the mean FA in every slice along the major axis of each tract (coronal slices for tracts which project anterior/posterior; axial slices for tracts which project dorsal/ventral). In individually traced tracts, average FA was calculated by taking the mean FA in all masked voxels. In the probabilistic atlas, the FA was weighted by the probability in each voxel using:

$$\mathrm{FA} = \frac{\sum_i \mathrm{FA}_i \times P_i}{\sum_i P_i} \tag{1}$$

where FA_i is the FA in voxel i and P_i is the probability in voxel i. The Pearson correlation coefficient was then calculated between the probabilistic FA and individual FA. The average FA over the whole tract was also calculated for both probabilistic and individual tracts. The correlation, over all tracts, between probabilistic and individual measurements was assessed. Bland-Altman plots (Altman and Bland, 1983) were also constructed to compare the precision and accuracy of whole-tract FA measured by the atlas with individually traced measurements. The same methods were also applied to the JHU atlas for comparison.

Whole-tract correlation plots and Bland-Altman plots were constructed for the 7 ABIDE subjects to assess the generalisation of the age-specific atlas. This is a deliberately conservative test due to the different age range and suboptimal tractography algorithm (see Section 4, Discussion). Validation of the volumetric overlap and slice-wise correlations for the ABIDE subjects are also provided in the supplementary materials for completeness.

2.6 Case Study

As a demonstration, the age-specific atlas produced here was used to investigate tract-level differences in white matter microstructure between the case and control children of the CoolMRI study. In all the tracts delineated by the age-specific atlas, the average FA in the tract was calculated for each individual using Equation 1. Bilateral tracts were tested separately. Mann-Whitney U tests were applied to test for differences in the median FA between cases and controls in each tract, with Bonferroni correction applied to correct for family-wise error. Significant results have corrected $p < 0.05$. For comparison, the equivalent analysis was performed using the adult-derived JHU atlas. In the absence of "ground-truth", only a qualitative comparison of results obtained with the two atlases was performed.

3 Results

3.1 Participant Demographics

The CoolMRI study recruited 51 children, without CP, treated with TH for NE at birth and 43 control children matched for age, sex and SES (Lee-Kelland et al., 2020). Of the recruited children, 7 cases and 4 controls did not want to undergo scanning. A further 4 cases had incomplete data due to movement during the scan. Quality control (Section 2.3) led to the rejection of a further 6 cases and 2 controls. One further case and one control were rejected due to incorrect image volume placement. This left 33 cases and 36 controls. These controls were split into 28 (15 M) for atlas construction and 8 (4 M) for validation. Data for each set of participants is shown in Table 1.

	Atlas Data			TH Data		
	Atlas (n = 28)	Validation (n = 8)	p	Cases (n = 33)	Controls (n = 36)	p
Age	7.0 (6.1-7.9)	7.0 (6.1-7.8)	0.9392	6.9 (6.0-7.9)	7.0 (6.1-7.9)	0.5595
SES	B (A-D)	B (A-C1)	0.7305	C1 (A-E)	B (A-D)	0.1568
M/F	15/13	4/4	0.8776	18/15	19/17	0.8894
FSIQ	108 (75-127)	112.5 (88-137)	0.3032	93 (62-115)	108 (75-137)	<0.0001

Table 1: Demographics of participants in the atlas and validation dataset, and in the TH dataset. Mean (range) is shown for age; Median (range) is shown for SES and FSIQ. SES is defined as follows: A= upper middle class, B = middle class, C1 = lower middle class, C2 = skilled working class, D = working class.

3.2 Atlas

Figure 4 shows the probabilistic map for each tract, as well as the aDWI and FA images for the group of 28 children.

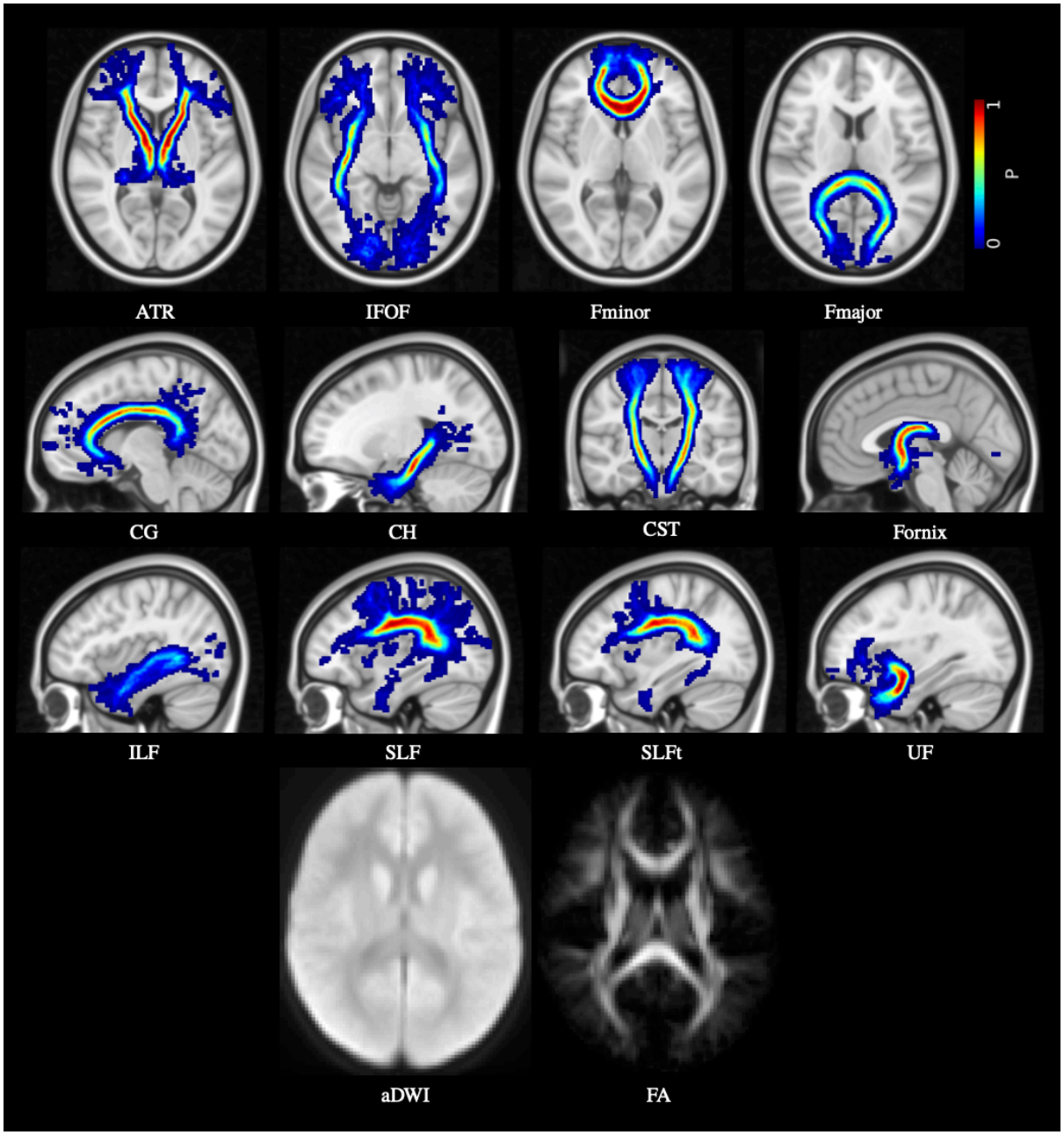

Figure 4: Age-specific probabilistic atlas for the 12 major white matter tracts: anterior thalamic radiation (ATR); inferior fronto-occipital fasciculus (IFOF); forceps minor (Fminor); forceps major (Fmajor); cingulate gyrus part of the cingulum (CG); hippocampal part of the cingulum (CH); cortico-spinal tract (CST); fornix; inferior longitudinal fasciculus (ILF); superior longitudinal fasciculus (SLF); temporal part of the superior longitudinal fasciculus (SLFt); and uncinate fasciculus (UF). Probabilities are indicated by the colour bar. Also shown are the aDWI and FA maps.

3.3 Validation

3.3.1 Volumetric Overlap

The Dice score at a range of thresholds is plotted for each tract for the same-site data in Figure 5, and the ABIDE data in Figure S1. In the same-site validation data, the peak of the median Dice score for the age-specific atlas is higher than for the JHU atlas in every tract. In the ABIDE data, though the difference is smaller, the peak of the median Dice score for the age-specific atlas is higher than for the JHU atlas in all tracts apart from the Fmajor and CST and SLF.

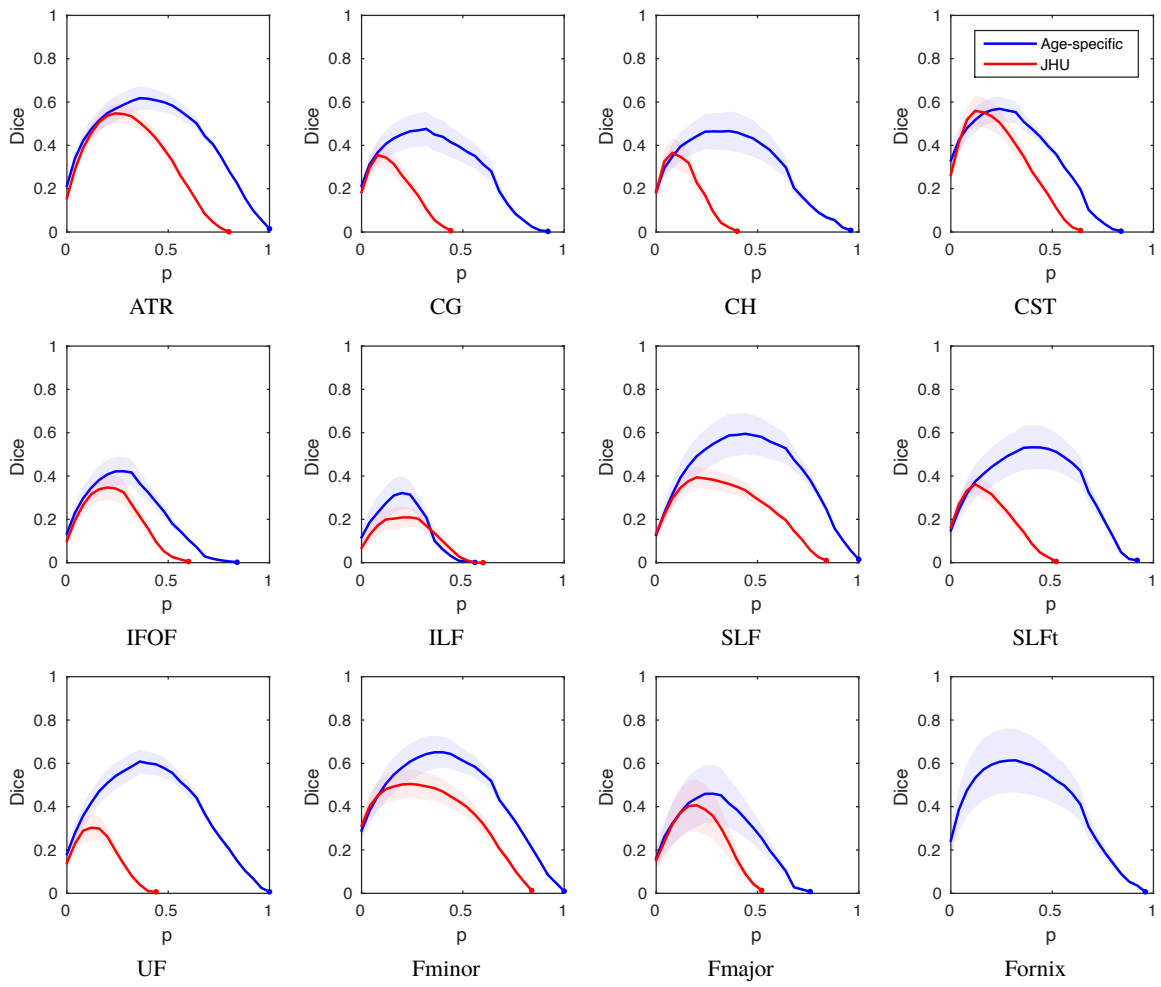

Figure 5: Same-site validation of tract overlap with "gold-standard" subject specific tract tracing. Plots show the Dice score of volumetric overlap (y axis) against probability threshold (x axis) when using the age-specific atlas (blue) or the JHU adult atlas (red), plotted up to the threshold at which no voxels remain. Lines show the median score for the 8 validation subjects not included in the formation of the atlas, and shaded regions show the 95% confidence interval. Note that the age-specific atlas (derived from data acquired on the same scanner, but different subjects), outperformed

the JHU (adult) atlas in all tracts. The tract representing the fornix is not available in the JHU atlas so only the new mask was tested.

3.3.2 DWI Metrics

The correlation between FA in slices measured by the age-specific atlas and individual tracing is shown for the same-site validation data in Figure 6, with correlation coefficients given in Table S1 and Figure S2. The correlation for the ABIDE data is shown in Figure S3, with coefficients given in Table S2 and Figure S4. Better agreement between the "gold-standard" (i.e. individual tract tracing) and the FA estimated from the different atlases (age-specific or JHU) is reflected by slopes closer to one, and smaller spread of data around this line. In the same-site data, most tracts show strong correlation between FA measured by the age-specific atlas and that measured by tracing in the individual, with all tracts having $r > 0.8$ apart from the CG ($r = 0.60$), SLF ($r = 0.50$) and SLFt ($r = 0.54$). In the ABIDE data, seven of the twelve tracts have $r > 0.7$, with the exception of the CG ($r = 0.67$), CH ($r = 0.62$), SLF ($r = 0.66$), SLFt ($r = 0.51$) and UF ($r = 0.69$). The age-specific atlas almost always performs better than the JHU atlas; in the same-site validation, every tract exhibits higher correlation when delineated with the age-specific atlas than with the JHU atlas, and in the ABIDE data this is the case for all tracts apart from the SLF (age-specific $r = 0.66$; JHU $r = 0.70$), the IFOF (for which both atlases give the same correlation, $r = 0.88$) and the CST (for which both atlases give the same correlation, $r = 0.89$).

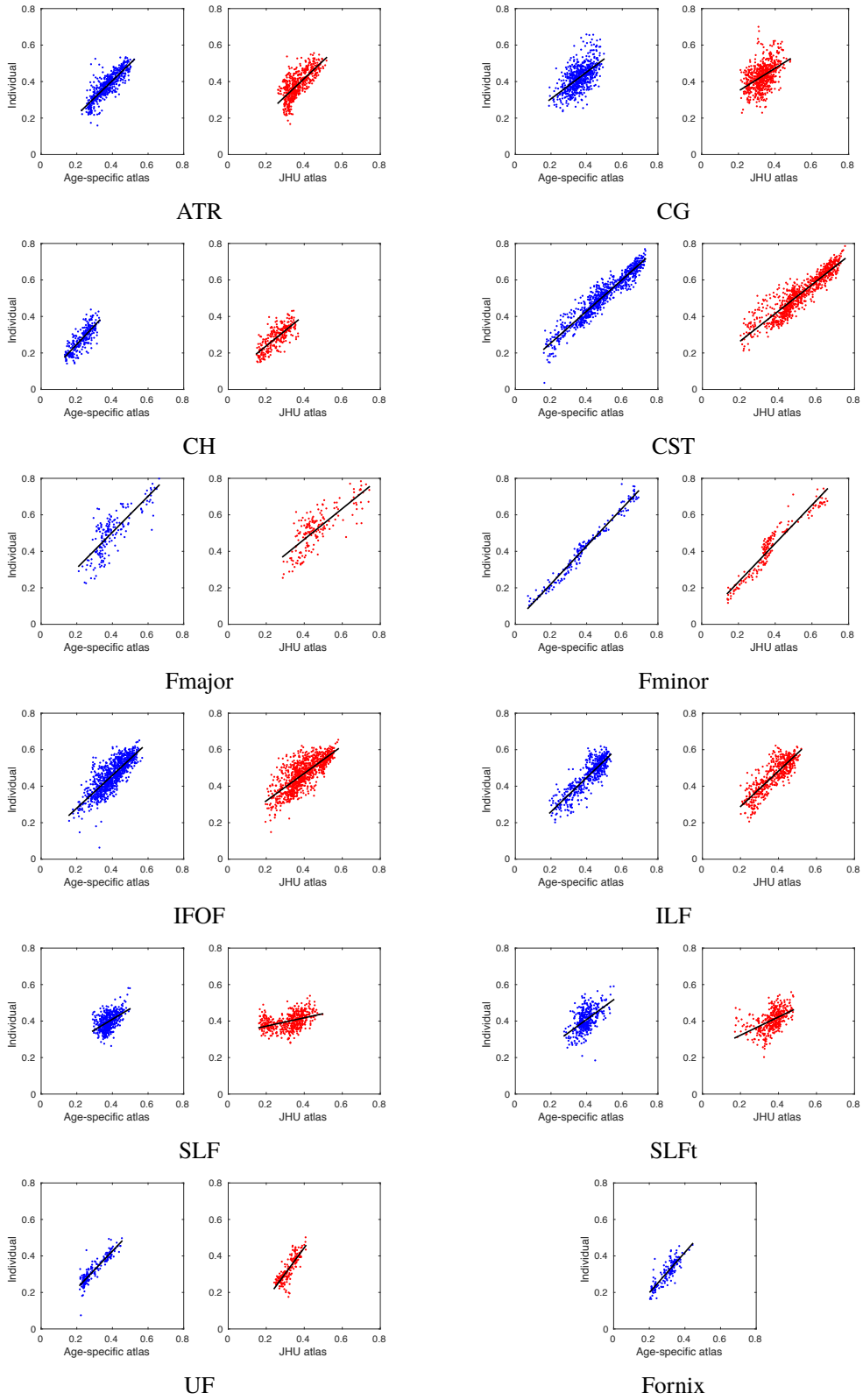

Figure 6: Same-site validation of slice FA values. Plots show slice FA measured from individually traced tracts (i.e. the "gold-standard") plotted against corresponding values extracted from the age-specific and JHU atlases. Each plot shows a point for every slice in each of the 8 validation subjects and the regression.

The whole-tract FA measured by the atlas is plotted against that given by tracing in individuals in Figure 7 and Bland-Altman plots are shown in Figure 8. The fornix is not included in these plots to allow valid comparison with the JHU atlas. For both the same-site and ABIDE validation data, the regression to the age-specific atlas measurements has slope closer to unity and intercept closer to zero than the JHU atlas (see Figure 7). The age-specific atlas also shows stronger correlation than the JHU atlas for both same-site data (age-specific r = 0.72; JHU r = 0.54) and ABIDE data (age-specific r = 0.75; JHU r = 0.72). Both the age-specific atlas and the JHU atlas have a positive bias compared to the individual measurements in the same-site and ABIDE data. Considering the Bland-Altman plots (Figure 8), the age-specific atlas has narrower limits of agreement (LOA) than the JHU atlas in both the same-site and ABIDE data.

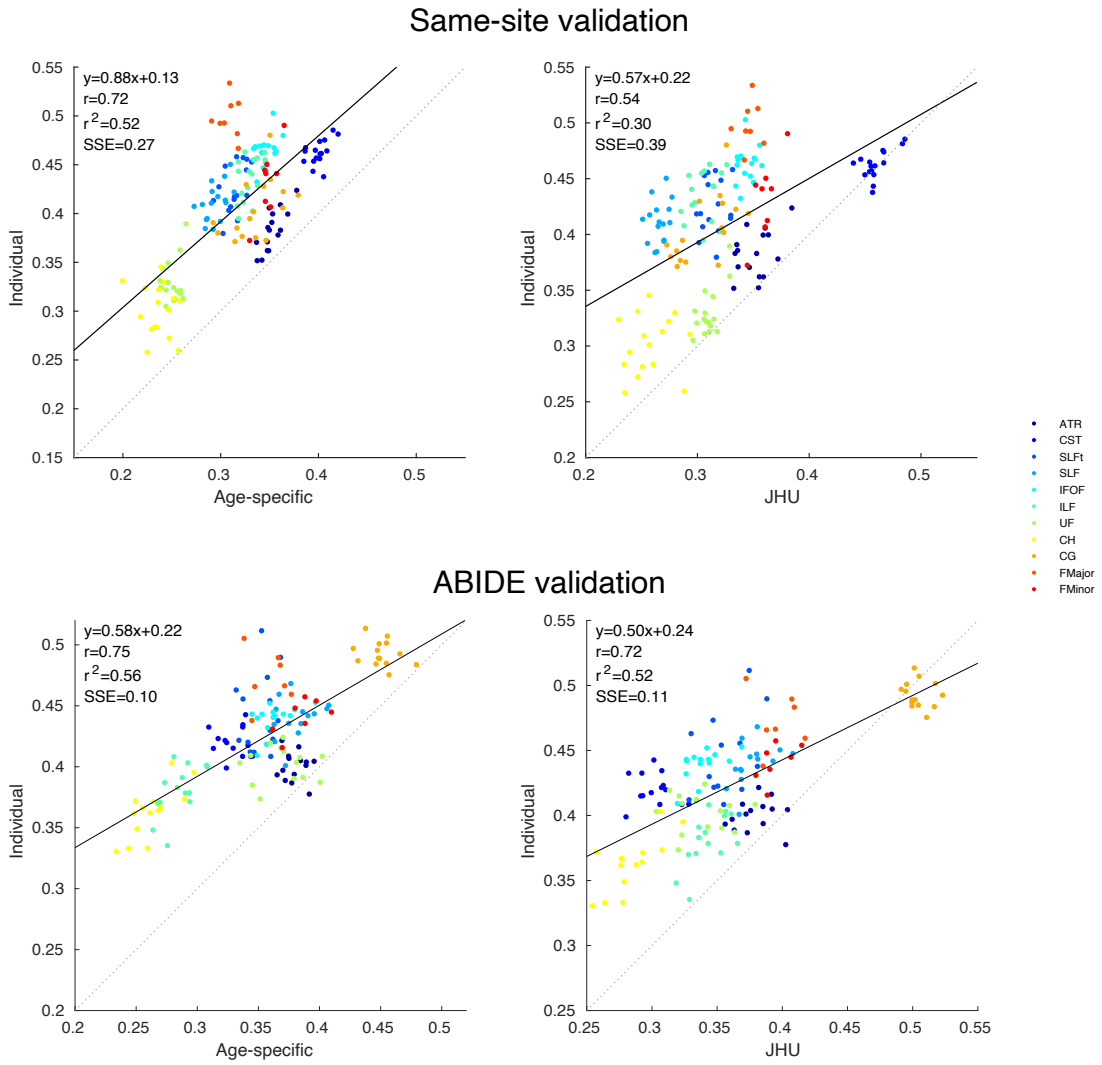

Figure 7: Comparison of mean FA extracted from whole tracts traced in individuals ("gold-standard") and that estimated using the age-specific or JHU (adult) atlases. FA in individually traced tracts is plotted against tract FA measured by the probabilistic atlases for same-site data (top row) and ABIDE data (bottom row). The solid line shows the regression, and the dotted line represents exact

equality between individual and the age-specific or JHU data. Displayed on each plot is the slope and intercept equation, the Pearson correlation coefficient, r, the squared Pearson correlation coefficient, r^2, and the sum of squared error (SSE).

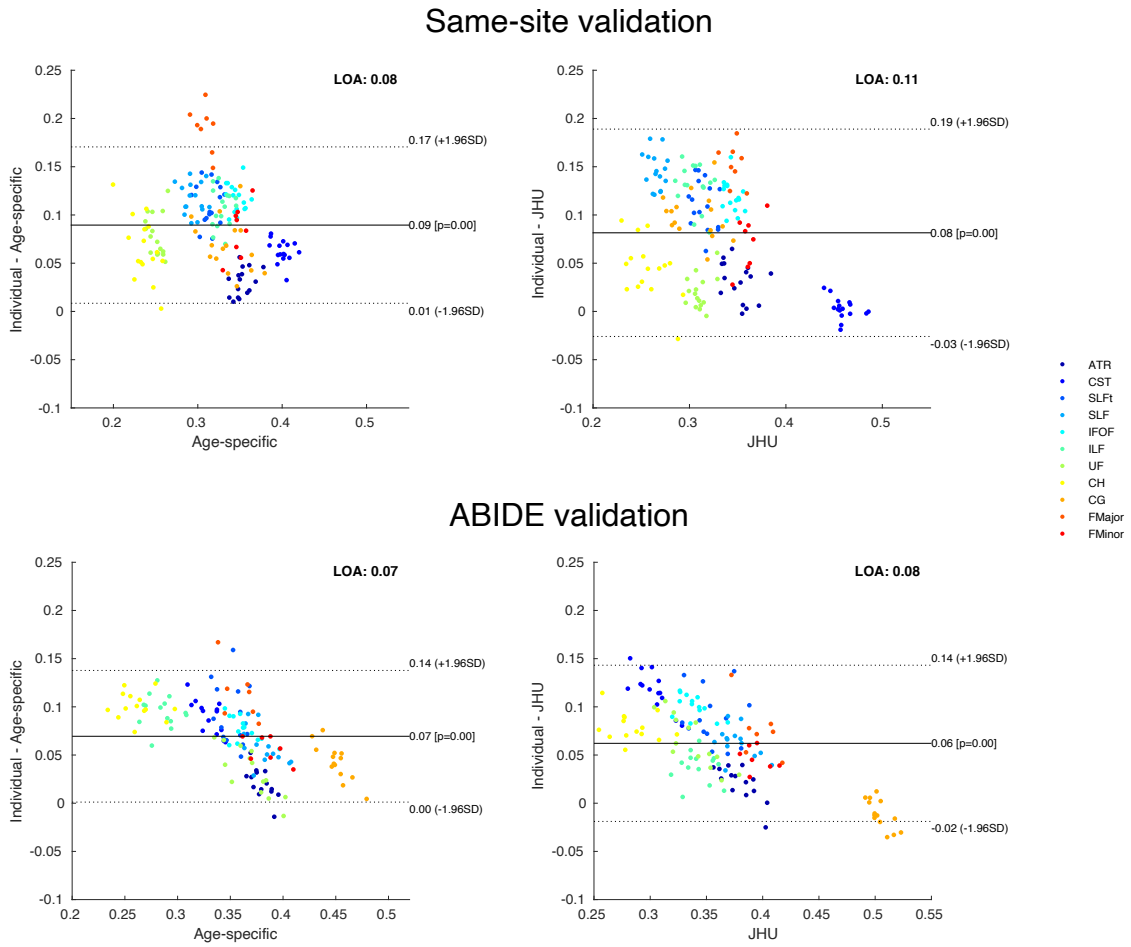

Figure 8: Bland-Altman plots for whole-tract average FA measurements in same-site data (top row) and ABIDE data (bottom row), plotted for both the age-specific atlas (left) and JHU atlas (right). The limits of agreement (LOA) are shown on each plot.

3.4 Case Study

Numerous tracts in children treated with TH for NE have reduced FA compared to controls (see Table S3). After Bonferroni correction, only the left CG ($p = 0.0056$), left CH ($p = 0.0081$), left SLF ($p = 0.0383$), and fornix ($p = 0.0121$) have significantly reduced FA in cases compared to controls. Box plots for these tracts are shown in Figure 9.

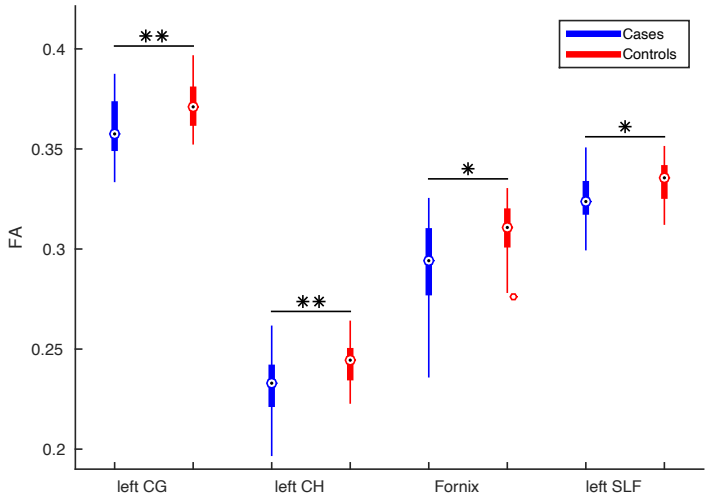

Figure 9: Box plots of significant differences in whole-tract average FA between children treated with TH for NE and healthy controls. *p < 0.05 **p<0.01, Bonferroni corrected.

The same analysis was run with the JHU atlas for comparison (see Table S4). Three tracts which were significant before Bonferroni correction when measured using the age-specific atlas, were not significant with the JHU atlas. Additionally, the left SLF, which was significant after correction when measured with the age-specific atlas, did not survive correction when measured with the JHU atlas. The left CG was significant with both atlases after correction; however, the p-value was lower when measured with the age-specific atlas. The left CH was significant after correction when measured with both atlases and was slightly more significant when measured with the JHU atlas. The right CH was significant after correction when measured with the JHU atlas but not the age-specific atlas. The fornix was significant when measured with the age-specific atlas but is not available in the JHU atlas so could not be tested.

4 Discussion

This study introduces an age-specific probabilistic white matter atlas constructed from children aged 6-8 years, providing a method of delineating white matter tracts in younger cohorts who may be averse to the long scanning times required for tractography based on HARDI data. We have shown that this atlas accurately delineates tracts in children from a same-site cohort aged 6-8 years, and a cohort from a different site, imaged with different scanner and acquisition protocol, aged 8-9 years. The strong correlation between FA sampled by the atlas and that measured in each individual (i.e. the "gold-standard"), at both a whole-tract level and slice-wise level, shows that the atlas provides an accurate estimate for the underlying white matter microstructure. Additionally, the high Dice scores between tracts in the age-specific atlas and those delineated by tractography in each validation

individual demonstrate a high level of volumetric overlap (indicating improved anatomical accuracy of the age-specific atlas). In both measures of validation, the age-specific atlas almost always performs better than simply registering to an existing adult white matter tract atlas, as is routinely done in the literature. As proof of concept, we applied the age-specific atlas to the CoolMRI study, revealing significantly reduced FA in several major white matter tracts in children treated with TH for NE at birth compared to healthy controls.

The correlation of whole-tract FA measured by the atlas with that given by individual tracing offers quantification of the performance of the atlas as a whole. In both the same-site validation data and the ABIDE validation data, the age-specific atlas exhibits stronger correlation with the individual measurements, with the slope of the regression closer to unity, than for the JHU atlas. The narrower limits of agreement in the Bland-Altman plots and higher correlation coefficient for the age-specific atlas indicate that this has higher precision than the JHU atlas. The strong correlation and high precision of diffusion metrics sampled by the age-specific atlas shows that this can characterise the distribution of tract-level diffusion metrics in a study group, facilitating more sensitive group comparison and investigation of associations between these metrics and neuropsychological and behavioural measures.

Those tracts which exhibit a lower correlation between atlas and individual slice-wise FA measurements (namely the CG, SLF and SLFt, as well as the CH and UF in the ABIDE data) have very little spread in FA values, resulting in tightly grouped measurements with a low correlation coefficient, as shown in Figures 6 and S3. For these tracts, the Dice scores in Figures 5, as well as the tract-wise validation in Figures 7 and 8 demonstrate improved performance of the age-specific atlas on the level of whole tracts.

Long, thin tracts, such as the CST, IFOF and ILF, are particularly susceptible to partial volume effects when measuring overlap; a small radial translation will result in a large change to the Dice score. In these tracts, the high correlation in sampled FA values shows that the age-specific atlas gives accurate measurement of the tract microstructure.

Multi-site validation alleviates bias associated with using the same scanner for validation data and atlas construction. The age range of the ABIDE validation data is slightly higher than that of the atlas data, simply due to data availability, however the age-specific atlas still performs better than that obtained from adults i.e. the JHU atlas. Further bias may be introduced by the use of the same tractography algorithm in atlas creation and the same-site validation data, thus a different tractography algorithm was used for the ABIDE data, such that the results and conclusions drawn from them are deliberately conservative. Whereas the FOD-based algorithm used to construct the age-specific atlas uses spherical deconvolution to find the peak FOD in the closest orientation to the propagating

streamline, the tensor-based algorithm used for the ABIDE data propagates the streamline along the principal eigenvector of the diffusion tensor at each step, similar to the tensor-based fibre tracking algorithm used in the construction of the JHU atlas. Despite this bias towards the JHU atlas, the age-specific atlas still performed better overall in the ABIDE validation.

This introduces the question of how to provide the "gold-standard" of fibre tracking; the tensor-based algorithm was used for the ABIDE data in order to eliminate bias towards the age-specific atlas, however this category of fibre tracking algorithm is widely acknowledged to give poor characterisation of diffusion in brain white matter due to its inability to resolve crossing fibres (Behrens et al., 2007; Tournier et al., 2012). Thus, the FOD-based algorithm used in the construction of the atlas and in the same-site validation data, which facilitates more comprehensive tracing due to its superior performance in regions of crossing fibres (Tournier et al., 2008), arguably gives a more accurate representation of the ground truth (i.e. the underlying white matter fibres). Therefore, when inspecting the volumetric overlap between the atlas and individually traced tracts in the validation data, the same-site data traced with the FOD-based algorithm likely gives a better indication of performance overall. Consequently, we believe the ABIDE validation provides a worst-case performance estimate – the fibre tracking algorithm is comparable to the JHU atlas and the age range is above that of the age-specific atlas – yet the age-specific atlas still out-performs the adult JHU atlas.

In future, as well as providing coverage of other age ranges, atlases could offer more extensive labelling of additional tracts and regions of white matter. A comprehensive database of traced tracts across a range of ages, potentially constructed by applying automated tractography-based white matter tract segmentation protocols (Lawes et al., 2008; Verhoeven et al., 2009; Wassermann et al., 2010; Zhang et al., 2018) to data from population studies such as the Human Connectome Project (Van Essen et al., 2013), Developing Human Connectome Project (Hughes et al., 2017), or Baby Connectome Project (Howell et al., 2019), would allow study-specific atlases to be built from subjects matched to a given study cohort.

Applying the age-specific atlas to the CoolMRI study to investigate group differences in tract-level FA revealed selective reduction in FA, that was significantly reduced in the left CG, left CH, left SLF and the fornix. The differences in the left CG were more significant when measured with the age-specific atlas than with the JHU atlas, and the differences in the left SLF are only significant with the age-specific atlas. Additionally, several tracts which are significant before Bonferroni correction when measured with the age-specific atlas are not significant with the JHU atlas. These results may indicate improved sensitivity of the age-specific atlas facilitating more accurate measurements of the distribution of FA values in each group. Differences in the right CH were significant when measured with the JHU but not the age-specific atlas. The improved performance of the age-specific atlas in the

volumetric overlap and slice-wise correlation of the CH suggests that this may be a false positive when measured with the JHU atlas. This comparison between the group differences revealed by each atlas highlights the benefits of improved sensitivity when applying the atlas to a patient cohort. However, it is important to recognise that in the absence of "ground truth" these comparisons are qualitative in nature, and do not provide definitive evidence to support the use of one atlas over another.

Previous studies of neonates treated with TH for NE have investigated the relationship between white matter diffusion properties, measured in the first weeks following birth, and neurodevelopmental outcome at 2 years of age. These studies found a significant reduction in FA in infants with adverse outcomes, compared to those with favourable outcomes, in widespread areas of white matter including, but not limited to the corpus callosum, anterior and posterior limbs of the internal capsule, external capsule, fornix, cingulum, and ILF (Lally et al., 2019; Tusor et al., 2012). Many of these regions were also shown to have reduced FA in the CoolMRI cases, indicating that the early structural alterations resulting from the brain injury cause lasting changes to white matter development. These results also provide evidence for an underlying white matter deficit which manifests as neuropsychological differences seen at school-age (Jary et al., 2019; Lee-Kelland et al., 2020; Tonks et al., 2019). Further investigation is required to link these structural impairments to specific components of the cognitive and motor assessments, and to develop possible therapeutic intervention strategies.

5 Conclusions

The age-specific atlas provided by this study has been shown to robustly delineate white matter tracts in children aged 6-8 years. Diffusion metrics sampled by the atlas correlate strongly with those measured by individual fibre tracking, allowing reliable investigation of white matter microstructure in cohorts where running tractography in every individual may not be an option.

Acknowledgements

We thank the children and their families for participating, Jade Thai for the assistance with MR sequences, Aileen Wilson for her radiographical expertise, and James Tonks, Charlotte Whitfield and Emily Broadbridge for their assistance with neuropsychological assessment.

Funding

This work was supported by the Baily Thomas Charitable Fund [grant number TRUST/VC/AC/SG4681-7596]. AS is supported by the Wellcome Trust [grant number

220070/Z/20/Z]. JCWB is supported by the UK Medical Research Council [grant number MR/N026969/1]. Funding sources had no role in study design; in the collection, analysis and interpretation of data; in the writing of the report; and in the decision to submit the article for publication.

References

Altaye, M., Holland, S.K., Wilke, M., Gaser, C., 2008. Infant brain probability templates for MRI segmentation and normalization. Neuroimage 43, 721–730. https://doi.org/10.1016/J.NEUROIMAGE.2008.07.060

Altman, D.G., Bland, J.M., 1983. Measurement in Medicine: The Analysis of Method Comparison Studies. Stat. 32, 307. https://doi.org/10.2307/2987937

Ameis, S.H., Catani, M., 2015. Altered white matter connectivity as a neural substrate for social impairment in Autism Spectrum Disorder. Cortex 62, 158–181. https://doi.org/10.1016/j.cortex.2014.10.014

Andersson, J.L.R., Jenkinson, M., Smith, S., 2007. Non-linear registration aka spatial normalisation [WWW Document]. FMRIB Tech. Rep. TRO7JA2. URL http://fmrib.medsci.ox.ac.uk/analysis/techrep/tr07ja2/tr07ja2.pdf

Andersson, J.L.R., Skare, S., Ashburner, J., 2003. How to correct susceptibility distortions in spin-echo echo-planar images: application to diffusion tensor imaging. Neuroimage 20, 870–888. https://doi.org/10.1016/S1053-8119(03)00336-7

Andersson, J.L.R., Sotiropoulos, S.N., 2016. An integrated approach to correction for off-resonance effects and subject movement in diffusion MR imaging. Neuroimage 125, 1063–1078. https://doi.org/10.1016/J.NEUROIMAGE.2015.10.019

Arrigoni, F., Peruzzo, D., Gagliardi, C., Maghini, C., Colombo, P., Iammarrone, F.S., Pierpaoli, C., Triulzi, F., Turconi, A.C., 2016. Whole-Brain DTI Assessment of White Matter Damage in Children with Bilateral Cerebral Palsy: Evidence of Involvement beyond the Primary Target of the Anoxic Insult. Am. J. Neuroradiol. 37, 1347–1353. https://doi.org/10.3174/ajnr.A4717

Asato, M.R., Terwilliger, R., Woo, J., Luna, B., 2010. White matter development in adolescence: A DTI study. Cereb. Cortex 20, 2122–2131. https://doi.org/10.1093/cercor/bhp282

Assaf, Y., Johansen-Berg, H., Thiebaut de Schotten, M., 2019. The role of diffusion MRI in neuroscience. NMR Biomed. 32, e3762. https://doi.org/10.1002/nbm.3762

Assaf, Y., Pasternak, O., 2008. Diffusion Tensor Imaging (DTI)-based White Matter Mapping in Brain Research: A Review. J. Mol. Neurosci. 34, 51–61. https://doi.org/10.1007/s12031-007-0029-0

Basser, P.J., Pajevic, S., Pierpaoli, C., Duda, J., Aldroubi, A., 2000. In vivo fiber tractography using DT-MRI data. Magn. Reson. Med. 44, 625–632. https://doi.org/10.1002/1522-2594(200010)44:4<625::AID-MRM17>3.0.CO;2-O

Bastiani, M., Andersson, J.L.R., Cordero-Grande, L., Murgasova, M., Hutter, J., Price, A.N., Makropoulos, A., Fitzgibbon, S.P., Hughes, E., Rueckert, D., Victor, S., Rutherford, M., Edwards, A.D., Smith, S.M., Tournier, J.-D., Hajnal, J. V., Jbabdi, S., Sotiropoulos, S.N., 2019. Automated processing pipeline for neonatal diffusion MRI in the developing Human Connectome Project. Neuroimage 185, 750–763. https://doi.org/10.1016/J.NEUROIMAGE.2018.05.064

Behrens, T.E.J., Berg, H.J., Jbabdi, S., Rushworth, M.F.S., Woolrich, M.W., 2007. Probabilistic diffusion tractography with multiple fibre orientations: What can we gain? Neuroimage 34, 144–155. https://doi.org/10.1016/J.NEUROIMAGE.2006.09.018

Cascio, C.J., Gerig, G., Piven, J., 2007. Diffusion tensor imaging: Application to the study of the developing brain. J. Am. Acad. Child Adolesc. Psychiatry 46, 213–223. https://doi.org/10.1097/01.chi.0000246064.93200.e8

Dennis, E.L., Thompson, P.M., 2013. Typical and atypical brain development: a review of neuroimaging studies. Dialogues Clin. Neurosci. 15, 359–84.

Di Martino, A., O'Connor, D., Chen, B., Alaerts, K., Anderson, J.S., Assaf, M., Balsters, J.H., Baxter, L., Beggiato, A., Bernaerts, S., Blanken, L.M.E., Bookheimer, S.Y., Braden, B.B., Byrge, L., Castellanos, F.X., Dapretto, M., Delorme, R., Fair, D.A., Fishman, I., Fitzgerald, J., Gallagher, L., Keehn, R.J.J., Kennedy, D.P., Lainhart, J.E., Luna, B., Mostofsky, S.H., Müller, R.-A., Nebel, M.B., Nigg, J.T., O'Hearn, K., Solomon, M., Toro, R., Vaidya, C.J., Wenderoth, N., White, T., Craddock, R.C., Lord, C., Leventhal, B., Milham, M.P., 2017. Enhancing studies of the connectome in autism using the autism brain imaging data exchange II. Sci. Data 4, 170010. https://doi.org/10.1038/sdata.2017.10

Dice, L.R., 1945. Measures of the Amount of Ecologic Association Between Species. Ecology 26, 297–302. https://doi.org/10.2307/1932409

Dimond, D., Schuetze, M., Smith, R.E., Dhollander, T., Cho, I., Vinette, S., Ten Eycke, K., Lebel, C., McCrimmon, A., Dewey, D., Connelly, A., Bray, S., 2019. Reduced White Matter Fiber Density in Autism Spectrum Disorder. Cereb. Cortex 29, 1778–1788. https://doi.org/10.1093/cercor/bhy348

Fonov, V., Evans, A.C., Botteron, K., Almli, C.R., McKinstry, R.C., Collins, D.L., 2011. Unbiased average age-appropriate atlases for pediatric studies. Neuroimage 54, 313–327. https://doi.org/10.1016/j.neuroimage.2010.07.033

Griswold, M.A., Jakob, P.M., Heidemann, R.M., Nittka, M., Jellus, V., Wang, J., Kiefer, B., Haase, A., 2002. Generalized autocalibrating partially parallel acquisitions (GRAPPA). Magn. Reson. Med. 47, 1202–1210. https://doi.org/10.1002/mrm.10171

Hagmann, P., Sporns, O., Madan, N., Cammoun, L., Pienaar, R., Wedeen, V.J., Meuli, R., Thiran, J.-P., Grant, P.E., 2010. White matter maturation reshapes structural connectivity in the late developing human brain. Proc. Natl. Acad. Sci. 107, 19067–19072. https://doi.org/10.1073/pnas.1009073107

Horsfield, M.A., Jones, D.K., 2002. Applications of diffusion-weighted and diffusion tensor MRI to white matter diseases - a review. NMR Biomed. 15, 570–577. https://doi.org/10.1002/nbm.787

Howell, B.R., Styner, M.A., Gao, W., Yap, P.-T., Wang, L., Baluyot, K., Yacoub, E., Chen, G., Potts, T., Salzwedel, A., Li, G., Gilmore, J.H., Piven, J., Smith, J.K., Shen, D., Ugurbil, K., Zhu, H., Lin, W., Elison, J.T., 2019. The UNC/UMN Baby Connectome Project (BCP): An overview of the study design and protocol development. Neuroimage 185, 891–905. https://doi.org/10.1016/J.NEUROIMAGE.2018.03.049

Hua, K., Zhang, J., Wakana, S., Jiang, H., Li, X., Reich, D.S., Calabresi, P.A., Pekar, J.J., van Zijl, P.C.M., Mori, S., 2008. Tract probability maps in stereotaxic spaces: Analyses of white matter anatomy and tract-specific quantification. Neuroimage 39, 336–347. https://doi.org/10.1016/j.neuroimage.2007.07.053

Hughes, E.J., Winchman, T., Padormo, F., Teixeira, R., Wurie, J., Sharma, M., Fox, M., Hutter, J., Cordero-Grande, L., Price, A.N., Allsop, J., Bueno-Conde, J., Tusor, N., Arichi, T., Edwards, A.D., Rutherford, M.A., Counsell, S.J., Hajnal, J. V., 2017. A dedicated neonatal brain imaging system. Magn. Reson. Med. 78, 794–804. https://doi.org/10.1002/mrm.26462

Hüppi, P.S., Dubois, J., 2006. Diffusion tensor imaging of brain development. Semin. Fetal Neonatal Med. 11, 489–497. https://doi.org/10.1016/j.siny.2006.07.006

Jary, S., Lee-Kelland, R., Tonks, J., Cowan, F.M., Thoresen, M., Chakkarapani, E., 2019. Motor performance and cognitive correlates in children cooled for neonatal encephalopathy without cerebral palsy at school age. Acta Paediatr. Int. J.

Paediatr. 108, 1773–1780. https://doi.org/10.1111/apa.14780

Jenkinson, M., Bannister, P., Brady, M., Smith, S., 2002. Improved Optimization for the Robust and Accurate Linear Registration and Motion Correction of Brain Images. Neuroimage 17, 825–841. https://doi.org/10.1006/NIMG.2002.1132

Konrad, K., Eickhoff, S.B., 2010. Is the ADHD brain wired differently? A review on structural and functional connectivity in attention deficit hyperactivity disorder. Hum. Brain Mapp. 31, 904–916. https://doi.org/10.1002/hbm.21058

Lally, P.J., Montaldo, P., Oliveira, V., Soe, A., Swamy, R., Bassett, P., Mendoza, J., Atreja, G., Kariholu, U., Pattnayak, S., Sashikumar, P., Harizaj, H., Mitchell, M., Ganesh, V., Harigopal, Sundeep, Dixon, J., English, P., Clarke, P., Muthukumar, P., Satodia, P., Wayte, S., Abernethy, L.J., Yajamanyam, K., Bainbridge, A., Price, D., Huertas, A., Sharp, D.J., Kalra, V., Chawla, S., Shankaran, S., Thayyil, S., Lally, P.J., Montaldo, P., Oliveira, V., Soe, A., Swamy, R., Bassett, P., Mendoza, J., Atreja, G., Kariholu, U., Pattnayak, S., Sashikumar, P., Harizaj, H., Mitchell, M., Ganesh, V., Harigopal, Sundeeep, Dixon, J., English, P., Clarke, P., Muthukumar, P., Satodia, P., Wayte, S., Abernethy, L.J., Yajamanyam, K., Bainbridge, A., Price, D., Huertas, A., Sharp, D.J., Kalra, V., Chawla, S., Shankaran, S., Thayyil, S., 2019. Magnetic resonance spectroscopy assessment of brain injury after moderate hypothermia in neonatal encephalopathy: a prospective multicentre cohort study. Lancet Neurol. 18, 35–45. https://doi.org/10.1016/S1474-4422(18)30325-9

Lawes, I.N.C., Barrick, T.R., Murugam, V., Spierings, N., Evans, D.R., Song, M., Clark, C.A., 2008. Atlas-based segmentation of white matter tracts of the human brain using diffusion tensor tractography and comparison with classical dissection. Neuroimage 39, 62–79. https://doi.org/10.1016/J.NEUROIMAGE.2007.06.041

Lebel, C., Treit, S., Beaulieu, C., 2019. A review of diffusion MRI of typical white matter development from early childhood to young adulthood. NMR Biomed. 32, e3778. https://doi.org/10.1002/nbm.3778

Lebel, C., Walker, L., Leemans, A., Phillips, L., Beaulieu, C., 2008. Microstructural maturation of the human brain from childhood to adulthood. Neuroimage 40, 1044–1055. https://doi.org/10.1016/j.neuroimage.2007.12.053

Lee-Kelland, R., Jary, S., Tonks, J., Cowan, F.M., Thoresen, M., Chakkarapani, E., 2020. School-age outcomes of children without cerebral palsy cooled for neonatal hypoxic–ischaemic encephalopathy in 2008–2010. Arch. Dis. Child. - Fetal Neonatal Ed. 105, 8–13. https://doi.org/10.1136/archdischild-2018-316509

Moeller, S., Yacoub, E., Olman, C.A., Auerbach, E., Strupp, J., Harel, N., Uğurbil, K., 2010. Multiband multislice GE-EPI at 7 tesla, with 16-fold acceleration using partial parallel imaging with application to high spatial and temporal whole-brain fMRI. Magn. Reson. Med. 63, 1144–1153. https://doi.org/10.1002/mrm.22361

Phan, T.V., Smeets, D., Talcott, J.B., Vandermosten, M., 2018. Processing of structural neuroimaging data in young children: Bridging the gap between current practice and state-of-the-art methods. Dev. Cogn. Neurosci. 33, 206–223. https://doi.org/10.1016/j.dcn.2017.08.009

Richards, J.E., Sanchez, C., Phillips-Meek, M., Xie, W., 2016. A database of age-appropriate average MRI templates. Neuroimage 124, 1254–1259. https://doi.org/10.1016/J.NEUROIMAGE.2015.04.055

Sanchez, C.E., Richards, J.E., Almli, C.R., 2012. Age-specific MRI templates for pediatric neuroimaging. Dev. Neuropsychol. 37, 379–399. https://doi.org/10.1080/87565641.2012.688900

Setsompop, K., Cohen-Adad, J., Gagoski, B.A., Raij, T., Yendiki, A., Keil, B., Wedeen, V.J., Wald, L.L., 2012a. Improving diffusion MRI using simultaneous multi-slice echo planar imaging. Neuroimage 63, 569–580. https://doi.org/10.1016/j.neuroimage.2012.06.033

Setsompop, K., Gagoski, B.A., Polimeni, J.R., Witzel, T., Wedeen, V.J., Wald, L.L., 2012b. Blipped-controlled aliasing in parallel imaging for simultaneous multislice echo planar imaging with reduced g-factor penalty. Magn. Reson. Med.

67, 1210–1224. https://doi.org/10.1002/mrm.23097

Simmonds, D.J., Hallquist, M.N., Asato, M., Luna, B., 2014. Developmental stages and sex differences of white matter and behavioral development through adolescence: A longitudinal diffusion tensor imaging (DTI) study. Neuroimage 92, 356–368. https://doi.org/10.1016/J.NEUROIMAGE.2013.12.044

Smith, R.E., Tournier, J.-D., Calamante, F., Connelly, A., 2013. SIFT: Spherical-deconvolution informed filtering of tractograms. Neuroimage 67, 298–312. https://doi.org/10.1016/j.neuroimage.2012.11.049

Smith, S.M., Jenkinson, M., Woolrich, M.W., Beckmann, C.F., Behrens, T.E.J., Johansen-Berg, H., Bannister, P.R., De Luca, M., Drobnjak, I., Flitney, D.E., Niazy, R.K., Saunders, J., Vickers, J., Zhang, Y., De Stefano, N., Brady, J.M., Matthews, P.M., 2004. Advances in functional and structural MR image analysis and implementation as FSL. Neuroimage 23, S208–S219. https://doi.org/10.1016/J.NEUROIMAGE.2004.07.051

Sydnor, V.J., Rivas-Grajales, A.M., Lyall, A.E., Zhang, F., Bouix, S., Karmacharya, S., Shenton, M.E., Westin, C.-F., Makris, N., Wassermann, D., O'Donnell, L.J., Kubicki, M., 2018. A comparison of three fiber tract delineation methods and their impact on white matter analysis. Neuroimage 178, 318–331. https://doi.org/10.1016/j.neuroimage.2018.05.044

Tonks, J., Cloke, G., Lee-Kelland, R., Jary, S., Thoresen, M., Cowan, F.M., Chakkarapani, E., 2019. Attention and visuo-spatial function in children without cerebral palsy who were cooled for neonatal encephalopathy: a case-control study. Brain Inj. 33, 894–898. https://doi.org/10.1080/02699052.2019.1597163

Tournier, J.-D., Calamante, F., Connelly, A., 2013. Determination of the appropriate b value and number of gradient directions for high-angular-resolution diffusion-weighted imaging. NMR Biomed. 26, 1775–1786. https://doi.org/10.1002/nbm.3017

Tournier, J.-D., Calamante, F., Connelly, A., 2012. MRtrix: Diffusion tractography in crossing fiber regions. Int. J. Imaging Syst. Technol. 22, 53–66. https://doi.org/10.1002/ima.22005

Tournier, J.-D., Calamante, F., Connelly, A., 2007. Robust determination of the fibre orientation distribution in diffusion MRI: Non-negativity constrained super-resolved spherical deconvolution. Neuroimage 35, 1459–1472. https://doi.org/10.1016/j.neuroimage.2007.02.016

Tournier, J.-D., Smith, R., Raffelt, D., Tabbara, R., Dhollander, T., Pietsch, M., Christiaens, D., Jeurissen, B., Yeh, C.-H., Connelly, A., 2019. MRtrix3: A fast, flexible and open software framework for medical image processing and visualisation. Neuroimage 202, 116137. https://doi.org/10.1016/j.neuroimage.2019.116137

Tournier, J.-D., Yeh, C.-H., Calamante, F., Cho, K.-H., Connelly, A., Lin, C.-P., 2008. Resolving crossing fibres using constrained spherical deconvolution: Validation using diffusion-weighted imaging phantom data. Neuroimage 42, 617–625. https://doi.org/10.1016/J.NEUROIMAGE.2008.05.002

Tusor, N., Wusthoff, C., Smee, N., Merchant, N., Arichi, T., Allsop, J.M., Cowan, F.M., Azzopardi, D., Edwards, A.D., Counsell, S.J., 2012. Prediction of neurodevelopmental outcome after hypoxic–ischemic encephalopathy treated with hypothermia by diffusion tensor imaging analyzed using tract-based spatial statistics. Pediatr. Res. 72, 63–69. https://doi.org/10.1038/pr.2012.40

Van Essen, D.C., Smith, S.M., Barch, D.M., Behrens, T.E.J., Yacoub, E., Ugurbil, K., 2013. The WU-Minn Human Connectome Project: An overview. Neuroimage 80, 62–79. https://doi.org/10.1016/J.NEUROIMAGE.2013.05.041

Verhoeven, J.S., Sage, C.A., Leemans, A., Van Hecke, W., Callaert, D., Peeters, R., De Cock, P., Lagae, L., Sunaert, S., 2009. Construction of a stereotaxic DTI atlas with full diffusion tensor information for studying white matter maturation from childhood to adolescence using tractography-based segmentations. Hum. Brain Mapp. NA-NA. https://doi.org/10.1002/hbm.20880

Wakana, S., Caprihan, A., Panzenboeck, M.M., Fallon, J.H., Perry, M., Gollub, R.L., Hua, K., Zhang, J., Jiang, H., Dubey, P., Blitz, A., van Zijl, P., Mori, S., 2007. Reproducibility of quantitative tractography methods applied to cerebral white matter. Neuroimage 36, 630–644. https://doi.org/10.1016/j.neuroimage.2007.02.049

Wassermann, D., Bloy, L., Kanterakis, E., Verma, R., Deriche, R., 2010. Unsupervised white matter fiber clustering and tract probability map generation: Applications of a Gaussian process framework for white matter fibers. Neuroimage 51, 228–241. https://doi.org/10.1016/J.NEUROIMAGE.2010.01.004

Zhang, F., Wu, Y., Norton, I., Rigolo, L., Rathi, Y., Makris, N., O'Donnell, L.J., 2018. An anatomically curated fiber clustering white matter atlas for consistent white matter tract parcellation across the lifespan. Neuroimage 179, 429–447. https://doi.org/10.1016/J.NEUROIMAGE.2018.06.027